Site-Specific Photodecomposition in Conjugated Energetic Materials

Levi Lystrom,[†,‡] Yu Zhang,[†] Sergei Tretiak,[†] and Tammie Nelson*,[†]

[†]Theoretical Division, Physics and Chemistry of Materials (T-1), Los Alamos National Laboratory, Los Alamos, New Mexico 87545, United States

[‡]Department of Chemistry and Biochemistry, North Dakota State University, Fargo, North Dakota 58108-6050, United States

Ⓢ *Supporting Information*

ABSTRACT: Nonadiabatic excited-state molecular dynamics (NEXMD) has been used to study photodecomposition in a class of recently synthesized bicyclic conjugated energetic materials (CEMs) composed of fused tetrazole and tetrazine derivatives with increasing oxygen substitutions. Modification by oxygen functionalization has already been demonstrated to increase the two-photon absorption intensity in the target CEMs while simultaneously improving oxygen balance. Photodecomposition mechanisms in materials that undergo nonlinear absorption could be used to achieve controlled, direct optical initiation. Here, we use NEXMD simulations to model the nonradiative relaxation and photodecomposition in CEMs following photoexcitation by a simulated Nd:YAG laser pulse. Excess electronic energy is quickly converted into vibrational energy on a sub-100 fs time scale resulting in bond dissociation. We find that, for the studied tetrazine derivatives, the bicyclic framework is an important structural feature that enhances the photochemical quantum yield and the high atomic oxygen content increases the relaxation lifetime and opens additional photodissociation pathways targeting the oxygen-substituted sites. The presented analysis scheme based on bond orders in the swarm of NEXMD trajectories is a useful tool for determining photochemical reactions.
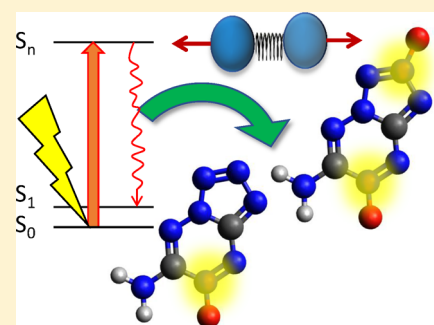
INTRODUCTION

In recent years, initiation of explosives using optical fibers has become widely recognized as a route toward improving performance and safety versus those of conventional electrical initiation.[1−5] However, current optical initiation techniques require high laser energies operating via indirect thermal or shock mechanisms. In contrast, direct optical initiation could occur through a photochemical pathway. In such a scenario, an optically active high explosive (HE) would undergo photodecomposition through an excited-state process as excess electronic energy is transferred to vibrational modes following photoexcitation.[6−8] A properly designed optically active HE with both linear and nonlinear two-photon absorption (TPA) would allow low-frequency and low-intensity light to be employed, offering greater control over the photochemical initiation mechanism.[9]

Conjugated energetic materials (CEMs) have emerged as promising candidates for photochemical direct optical initiation. Recently synthesized tetrazine- and tetrazole-based CEMs[10−13] have significant C−N and N−N content, giving them the advantage of high heats of formation and clean burning typically associated with high-nitrogen HEs while retaining the optical activity ubiquitous in conventional carbon-based conjugated materials. In fact, while most HEs are not photoactive and absorb only in the ultraviolet (UV) wavelength range, CEMs can have significant one-photon and TPA cross sections in the visible region that can be accessed by conventional lasers.[9]

Functionalization of HEs by addition of oxygen, NO_2, or NH_2 is often used to tune the oxygen balance and heat of formation to obtain the desired sensitivity and strength. It is well-known that functionalization of carbon-based conjugated organic materials can be used to tune the linear absorption and TPA response.[14,15] The same strategy has also been demonstrated in CEMs. Recent calculations of the TPA response in two classes of CEMs composed of different nitrogen-containing fused bicyclic frameworks with varying numbers of oxygen (O) and NO_2 substitutions have shown that addition of O increases the size of the TPA cross section while, at the same time, improves the oxygen balance.[9]

Here, nonadiabatic excited-state molecular dynamics (NEXMD) simulations are used to explore the relationship between functionalization and photochemical response in a series of previously studied tetrazine-based fused bicyclic CEMs that exhibit increased TPA responses upon addition of O substituents.[9] For the series of molecules, whose chemical structures are shown in Figure 1, the nonradiative relaxation from an initial high-energy electronic excited state and the subsequent photochemistry were modeled to study the possible enhancement of the photoactive response due to O addition and the bicyclic framework.
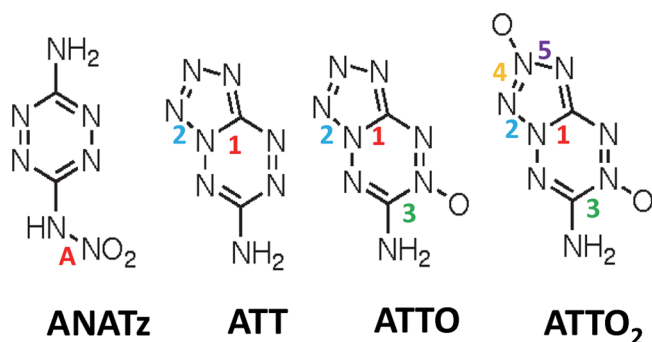
Figure 1. Chemical structures of N3-nitro-1,2,4,5-tetrazine-3,6-diamine (ANATz), tetrazolo[1,5-*b*][1,2,4,5]tetrazine-6-amine (ATT), and tetrazolo[1,5-*b*][1,2,4,5]tetrazine-6-amine with one (ATTO) and two (ATTO$_2$) O substitutions. Bonds involved in the initial photodissociation step are labeled.

■ COMPUTATIONAL DETAILS

NEXMD Overview. Nonadiabatic excited-state molecular dynamics (NEXMD) was used to model photoexcited dynamics in the CEMs shown in Figure 1. The underlying formalism of the NEXMD methodology is the same as the previously reported NAESMD. Details of the methodology can be found in our work.[16−21] Briefly, NEXMD is based on the mixed quantum classical fewest-switches surface hopping (FSSH) algorithm[22] allowing dynamics beyond the Born–Oppenheimer approximation to be followed as the system relaxes nonradiatively from a high-energy electronically excited state to the lowest-energy excited state. The classical nuclei evolve on a single adiabatic potential energy surface (PES) at any given time. The quantum mechanical description of electrons relies on analytically computed excited-state energies, gradients, and nonadiabatic couplings generated "on the fly".[16,23−26] The electronic and nuclear systems are coupled by stochastic-state switches in the PES for the nuclear trajectory based on the strength of the nonadiabatic coupling. In the NEXMD approach, the collective electronic oscillator (CEO) approach[27,28] is used to compute electronic excited states at the configuration interaction single (CIS)[29] level of theory with a semiempirical AM1[30] Hamiltonian. This approach retains essential electronic correlations (e.g., excitonic effects), and while it cannot describe states with significant double-excitation character,[31] it has the benefit of being able to treat excited-state dynamics in large conjugated systems and has been demonstrated to give a realistic description of tetrazine-based HEs.[6] Surface hopping simulations can be performed at various levels of theory, and many techniques for modeling photochemistry have been devised.[32−37] For our purposes, we require a description of nonradiative relaxation between multiple excited states in large molecular systems on the actual excited-state PESs. In the systems under study, photochemistry occurs on the excited state (rather than the ground state) after a high-energy photoexcitation. Time-dependent density functional theory and expensive multireference[38] or multiconfigurational[39] methods are significantly more numerically expensive for this task.

Solvent Model. All simulations of photochemical reactions were performed using linear-response solvation where the dynamics are coupled to the conductor-like polarizable continuum model (CPCM).[21,40−43] Briefly, this type of implicit solvent model treats the solvent as a dielectric continuum, which represents an average over many solvent configurations. The system of interest is embedded in a dielectric cavity[44] whose surface charge density is dictated by the charge density of the embedded molecule. The solvent response depends on the dielectric constant of the cavity, ε, through the induced polarization given by the equation $f(\varepsilon) = (\varepsilon - 1)/\varepsilon$.[45] The electrostatic potential produced by the surface charge distribution is added to the system Hamiltonian. For the present NEXMD simulations, a dielectric constant ε of 32.7 was used, corresponding to methanol. Simulations were also performed in vacuum ($\varepsilon = 1$) to determine the effect of the solvent on relaxation time scales and optical spectra. Because of its asymptotic form, the value of induced polarization $f(\varepsilon)$, and therefore the solvent effect, does not change significantly when $\varepsilon > 5$.[21]

Simulation Details. For each molecule, simulations were performed by first following ground-state (GS) molecular dynamics from the AM1-optimized geometry for 300 ps using a time step Δt of 0.5 fs and a friction coefficient of 20.0 ps^{-1} to equilibrate to 300 K using constant-temperature Langevin dynamics.[46] An ensemble of 500 initial geometries and momenta was collected from the GS trajectory, and for each configuration, the CEO method was used to compute oscillator strengths and vertical excitation energies for the 15 lowest-energy excited states. The equilibrated linear absorption spectra were made into a histogram of the excited-state energies in which the height is related to the average optical absorption at a given wavelength for the corresponding state. The initial excitation was chosen on the basis of a Franck–Condon window centered at 355 nm (see Results and Discussion) with a Gaussian temporal profile corresponding to a full width at half-maximum (FWHM) of 100 fs. The NEXMD simulations of isolated molecules were then started from the different photoexcited configurations and propagated independently using energy-conserving Newtonian dynamics. Constant-temperature Langevin dynamics was not performed for the excited-state dynamics under the assumption that photodecomposition requires sufficiently excited vibrational states to break bonds. Langevin dynamics would allow excess electronic energy to quickly dissipate to the bath, subject to the choice of empirical coefficient describing the viscosity of the solvent. This would reduce the excitation of vibrational states potentially preventing identification of the relevant decomposition pathways given the limited statistical sampling in terms of the number of trajectories simulated. Therefore, Newtonian dynamics was propagated for 1 ps with a classical time step Δt of 0.1 fs and a quantum time step δt of 0.033 fs where 15 excited states were included. The quantum time step was reduced by a factor of 10 to locate trivial unavoided crossings,[18] and the instantaneous decoherence correction[19] was included. The swarm of 500 trajectories allows the excited-state lifetimes and photochemical quantum yields to be computed as statistical averages. Further details about the computational protocol used here are reported elsewhere.[16−20]

Photochemistry Analysis. To analyze photochemical reactions, all interatomic distances are computed along the NEXMD trajectories and compared to bond-length thresholds, Δ_{ij}, determined on the basis of computed bond orders. The computed bond-length threshold will differ depending on whether a pair of atoms is initially bonded or nonbonded. MOPAC2016[47] is used to compute the bond order (BO) matrix corresponding to the ground-state AM1-optimized structure. Bond order is typically interpreted as a measure of

the bond covalency. A BO value of 0 corresponds to a purely ionic bond (or noncovalently bonded atoms), whereas a BO value of 1 would indicate a purely covalent two-electron bond. A non-integer value indicates a weak covalent bond.[48]

The bond order matrix is computed once for all trajectories; this is a valid approximation for all initial conditions because the ground-state adiabatic dynamics does not cause the formation or breaking of any bonds. This information is used to determine which atoms are initially bonded. The bond-length threshold is then set according to the following

$$\Delta_{ij} = \begin{cases} D_T + dx_{nb} & \text{if } BO_{ij} \geq 0.5 \\ D_T + dx_b & \text{if } BO_{ij} < 0.5 \end{cases} \quad (1)$$

where D_T is the tabulated bond length[49−51] and dx_{nb} and dx_b are parameters for nonbonded and bonded atoms set to 0.3 and 0.5 Å, respectively. The algorithm presented in Scheme 1

Scheme 1. Flowchart of Photochemical Pathway Analysis[a]
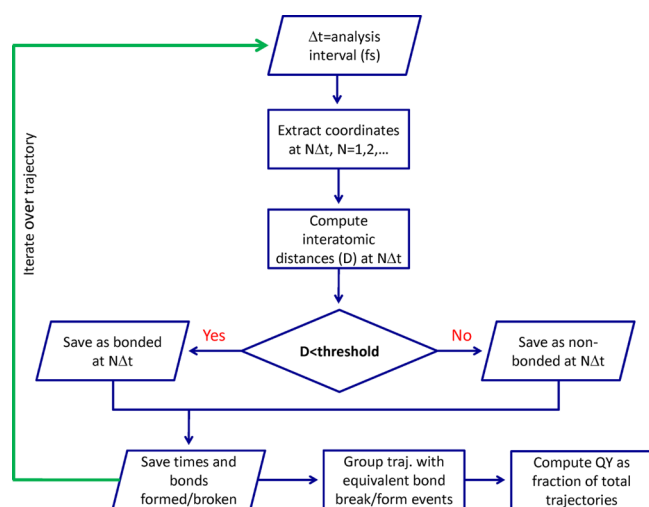
[a]For each specified time interval, all interatomic distances are compared to bond-dependent thresholds to identify bond breaking and formation events.

uses the bond-length threshold to find pairs of atoms with interatomic distances below (bonded) or above (nonbonded) the thresholds during dynamics. Trajectories that undergo the same sequence of bond cleavage and formation events are grouped within the same pathway, allowing quantum yields for individual pathways to be computed as the fraction of total trajectories in each group.

RESULTS AND DISCUSSION

The studied molecules, shown in Figure 1, are composed of unfunctionalized tetrazolo[1,5-*b*][1,2,4,5]tetrazine-6-amine (ATT) and analogues containing one (ATTO) and two (ATTO$_2$) O substitutions. We also include a single-tetrazine ring counterpart to ATT, N3-nitro-1,2,4,5-tetrazine-3,6-diamine (ANATz).

Optical Spectra. Experimental absorption spectra for the four compounds were obtained in 5 mM solutions of methanol and are shown in the top panel of Figure 2. The calculated one-photon equilibrated absorption spectra in methanol are shown in the bottom panel of Figure 2 computed with the AM1/CIS level of theory within the CEO framework. The
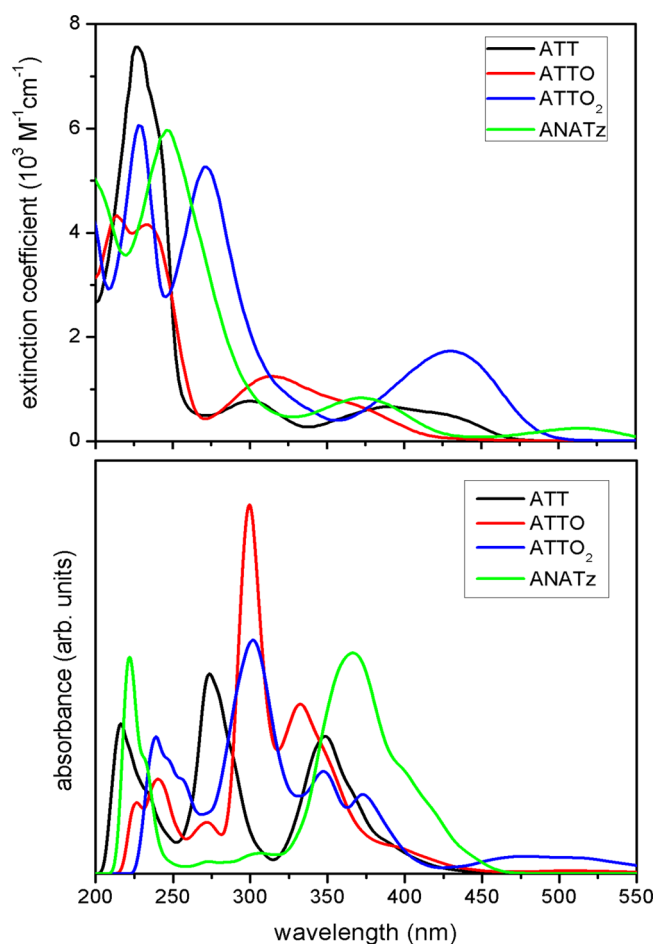

Figure 2. (Top) Experimentally determined extinction coefficients for the four compounds measured in 5 mM methanol solutions. (Bottom) Calculated one-photon equilibrated absorption spectra in methanol ($\varepsilon = 32.7$) at 300 K where the contributions of the 15 lowest-energy excited states are included.

computed spectra reveal maximum absorption energies that are similar among the bicyclic compounds, ranging from 275 to 300 nm. The values are slightly red-shifted compared to experimental maxima, which appear between 225 and 275 nm. Nevertheless, the chosen excitation wavelength of 355 nm, corresponding to an Nd:YAG laser harmonic, is aligned with the onset of the second absorption peak preceded by a broad low-intensity absorption feature at a lower energy in each system, consistent with the experimentally determined spectra.

The absorption spectra showing the contributions of individual excited states provided in Figure S1 reveal the effect of the polar solvent. The red shift of solvated spectra compared to vacuum calculations indicates a solvent stabilization effect that is most pronounced for S$_1$. The stabilization is enhanced in ATTO and ATTO$_2$ by the presence of electronegative oxygen, which increases the molecular dipole moment.

Excited-State Lifetimes and Relaxation Time Scales. Adiabatic-state populations (computed as the normalized fraction of trajectories) were fit to a three-state sequential irreversible kinetic model $A(t) \xrightarrow{k_1} B(t) \xrightarrow{k_2} C(t)$. In our model, $A(t)$ is the sum of the populations of all initially excited states, $B(t)$ is the sum of the intermediate-state populations, and $C(t)$ is the population of final state S$_1$. Because of conformational

disorder, a range of states are initially excited such that $A(t)$ corresponds to S_2-S_5 (ATT), S_3-S_8 (ATTO), S_5-S_{10} (ATTO$_2$), and S_3-S_6 (ANATz). For the few cases in which the initial excitation is created in S_1, the trajectory is removed from the ensemble. If S_2 is initially excited, then S_2 is incorporated into the initially excited $A(t)$ population and there is no intermediate state. Rate constants k_1 and k_2 are found by fitting the following equations

$$A(t) = e^{-k_1 t} \tag{2}$$

$$B(t) = \frac{k_1}{k_2 - k_1}(e^{-k_1 t} - e^{-k_2 t}) \tag{3}$$

$$C(t) = 1 - A(t) - B(t) \tag{4}$$

The evolutions of the state populations are shown in Figure 3 along with the fitted curves (dashes). The population is
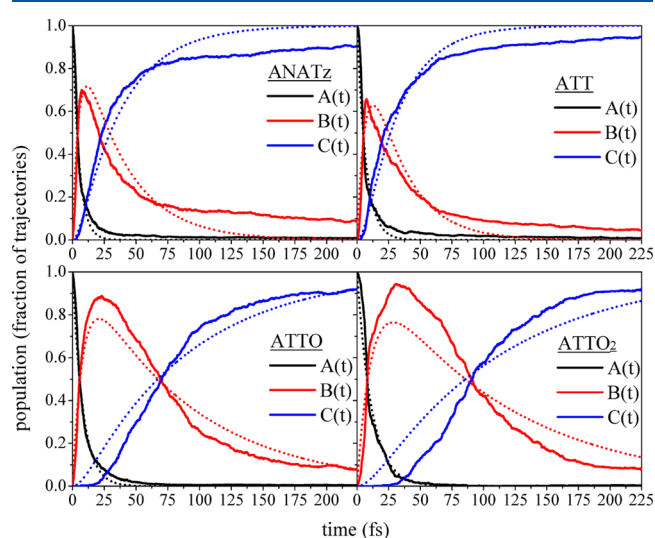

Figure 3. Time evolution of adiabatic-state populations during NEXMD simulations of the compounds in Figure 1 used for the three-state kinetic model (fit shown as dashes), where $A(t)$ represents the initial state, $B(t)$ values are intermediate states, and $C(t)$ is the final state. Time scales are listed in Table 1.

transferred from the initial state $[A(t)$, black curve$]$ to the lowest-energy S_1 state $[C(t)$, blue curve$]$ through a range of intermediate states $[B(t)$, red curve$]$ whose cumulative population increases and subsequently decays. The results of the fit are listed in Table 1, where $\tau_{ini} = 1/k_1$ represents the lifetime of the initial excited state and $\tau_{tot} = 1/k_1 + 1/k_2$ represents the total relaxation time scale. The initial excited-

Table 1. Results of Solvated Nonadiabatic Relaxation Dynamics, Including Excited-State Lifetimes and Relaxation Time Scales from the Three-State Sequential Kinetic Model and Average S_n-S_1 Energy Gaps and Total Photochemical Quantum Yields (QY)

	excited-state lifetime $\tau_{ini} = 1/k_1$ (fs)	relaxation time scale $\tau_{tot} = 1/k_1 + 1/k_2$ (fs)	average energy gap $\langle E_n - E_1 \rangle$ (eV)	total QY
ATT	6.9 ± 0.2	34.1 ± 0.4	0.5 ± 0.1	0.918
ATTO	8.1 ± 0.3	93.8 ± 0.6	1.2 ± 0.2	0.924
ATTO$_2$	11.4 ± 0.3	117.8 ± 0.8	1.4 ± 0.2	0.940
ANATz	5.2 ± 0.2	39.8 ± 0.5	0.6 ± 0.1	0.508

state lifetime is relatively unaffected by the addition of O, varying from 6.9 ± 0.2 fs in ATT to 8.1 ± 0.3 fs in ATTO and 11.4 ± 0.3 fs in ATTO$_2$. The initial excited-state lifetime in ANATz of 5.2 ± 0.2 fs is on the same ultrafast time scale as those of the bicyclic compounds. Comparison of the total nonradiative relaxation time scales for the four compounds reveals that the unsubstituted compounds ATT and ANATz, have similar and relatively fast time scales of 34.1 ± 0.4 and 39.8 ± 0.5 fs, respectively. The total relaxation is considerably slower for the O-substituted compounds. ATTO has a total relaxation time of 93.8 ± 0.6 fs, which is further increased to 117.8 ± 0.8 fs in ATTO$_2$.

The difference in relaxation times between ATT and ANATz is only 15%, while the relaxation time increases by 93% in ATTO and 110% in ATTO$_2$ compared to that of ATT, suggesting that the bicyclic framework does not affect the relaxation time scale as strongly as O functionalization. It is important to note that the addition of O to the bicyclic ring structure does not significantly change the initial excitation lifetime, as evidenced by the τ_{ini} values. Instead, O substitution causes the intermediate excited states to be longer-lived, resulting in a progressively slower overall relaxation process with each O addition.

The increase in total relaxation time is caused by larger energy gaps between excited states. Energy gap $\langle E_n - E_1 \rangle$, computed as the average difference in energy between initial excited state S_n and final state S_1, is shown in Table 1. The compounds with the smallest energy gaps, ATT and ANATz, have the fastest relaxation times. ATTO and ATTO$_2$ have larger energy gaps and therefore longer relaxation times because of the inverse relationship between nonadiabatic coupling strength (which is responsible for driving electronic relaxation) and the energy difference.

The calculated absorption spectra in Figure S1 reveal the contributions of individual states. The spectra show that the S_1 state is shifted to a lower energy (higher wavelength) in the O-substituted compounds, suggesting that the increased S_2-S_1 energy gap is the specific source of the bottleneck, as this gap becomes much larger while the density of states around 355 nm remains relatively unaffected. In the absence of solvent-induced stabilization of S_1, the S_n-S_1 energy gap is reduced (S_1 is at a higher energy) and relaxation time scales are faster, as confirmed by the data presented in Table S1 for simulations performed in vacuum.

Photodissociation Pathways and Quantum Yields. We next analyze the photochemical pathways, intermediate photoproducts, and photochemical quantum yields (QYs) of the four compounds. The photochemical QY is computed from NEXMD simulations as the fraction of trajectories that exhibit a particular bond breaking event. The relevant dissociation pathways can be distinguished by considering the first bond breaking event. Figure 4 summarizes the initial bond dissociation step for each compound and lists the corresponding quantum yield. The broken bonds are labeled according to Figure 1. The total photochemical QYs are listed in Table 1. Given the analysis of 500 trajectories, a small QY of <5% is not statistically meaningful and corresponds to rare events occurring in 25 or fewer trajectories. Movies of representative trajectories for each molecule demonstrating the primary initial bond cleavages described below are included with the Supporting Information.

The only photochemical pathway observed in NEXMD simulations of ANATz is the dissociation of NO$_2$ correspond-
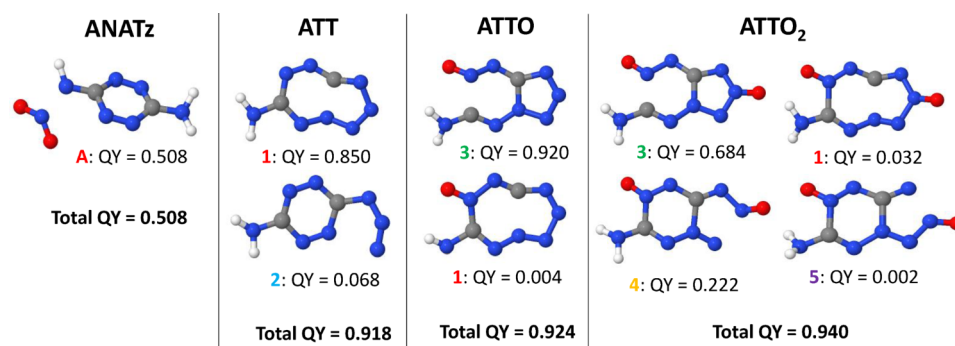
Figure 4. Initial bond breaking steps are shown for each compound along with the quantum yields. The bond numbers correspond to the labels in Figure 1. Quantum yields are computed as the fraction of total NEXMD trajectories that undergo the indicated bond cleavage as the initial step in dissociation.

ing to N−N bond cleavage of bond A (Figure 1) with a photochemical QY of 50.8%. Dissociation of the tetrazine ring was not observed, consistent with previous findings that functionalization stabilizes tetrazine.[6]

The primary photochemical pathway in ATT, the compound with the bicyclic framework with no O substitutions, is the cleavage of the fused ring by breaking the central C−N bond (bond 1 in Figure 1) to form a nine-membered ring. Ring expansion occurs in ATT with a QY of 85.0%. The secondary pathway in ATT is initiated by a cleavage of the N−N bond (bond 2 in Figure 1) to open the tetrazole ring, occurring with a QY of 6.8%. Both of the pathways proceed to release N≡N, as shown in Figure S2. However, the primary pathway produces a fragment with no ring, while the secondary pathway results in the preservation of the tetrazine ring. The total QY of ATT is 91.8%.

ATTO contains a bicyclic framework of fused tetrazine and tetrazole rings with an O functionalization on the tetrazine ring. Here the primary pathway of photodissociation begins with a cleavage of the tetrazine ring at the O-functionalized site where the C−N bond (bond 3 in Figure 1) is broken with a QY of 92.0%. The secondary pathway in ATTO is initiated by the same bond dissociation event as the primary pathway in ATT, specifically a ring expansion by breaking bond 1 to form the nine-membered ring. However, in ATTO, the ring expansion occurs with a much lower QY of 0.4% and the tetrazole ring (bond 2 in Figure 1) is not cleaved. The subsequent decomposition of ATTO, shown in Figure S3, results in the total destruction of the ring framework into multiple fragments or the preservation of the tetrazole. The total QY of ATTO is 92.4%.

ATTO$_2$ contains the same fused bicyclic framework as ATT and ATTO and has O functionalization on both the tetrazine and tetrazole rings. The primary pathway in ATTO$_2$ is again initiated by tetrazine cleavage at the O-substituted site (bond 3), identical to the primary initial photofragment in ATTO. However, the QY for the cleavage of bond 3 in ATTO$_2$ is reduced to 68.4%. The secondary pathway in ATTO$_2$ involves the cleavage of the tetrazole ring at the O-substituted site by breaking the N≡NO bond (bond 4) with a QY of 22.2%. The other N−NO bond (bond 5) on the tetrazole is a less favorable pathway and occurs with a QY of 0.2%, while the ring expansion by cleavage of bond 1, analogous to the pathways present in ATT and ATTO, contributes 3.2% to the total QY of 94.0%. As in ATTO, the opening of the tetrazole ring at the N−N site (bond 2 in Figure 1) does not occur in ATTO$_2$. The

subsequent dissociation pathways of ATTO$_2$ are shown in Figure S4, where several possible fragments form.

In summary, ring expansion (breaking of bond 1) occurs in all of the bicyclic compounds and is the dominant initial bond breaking event in ATT. In the O-substituted compounds, the competing pathway of ring opening at the O-substituted site (bond 3) of tetrazine becomes the primary pathway making the initial destruction of the tetrazine ring possible. The initial tetrazole ring cleavage at the N−N bond (bond 2) occurs only in ATT and is suppressed in ATTO and ATTO$_2$ in favor of N−NO and N≡NO (bonds 3−5) bond cleavage. For ATTO and ATTO$_2$, additional sites for cleavage appear as O is added, leading to more pathways and a slight increase in the photochemical quantum yield with each O addition.

■ CONCLUSION

Nonadiabatic excited-state molecular dynamics (NEXMD) simulations of four conjugated energetic materials have been performed to investigate their photochemical response as a function of O content. The series of compounds contain a fused tetrazine and tetrazole ring framework in either unfunctionalized form tetrazolo[1,5-b][1,2,4,5]tetrazine-6-amine (ATT) or O-substituted analogues containing one (ATTO) or two (ATTO$_2$) O atoms. A compound containing a single tetrazine ring, N3-nitro-1,2,4,5-tetrazine-3,6-diamine (ANATz), was also included to investigate the effect of the bicyclic framework on relaxation time scales and photochemical QYs. The simulated excitation was generated at 355 nm, consistent with Nd:YAG laser excitation.

We find that the addition of O to the bicyclic ring structure causes the overall electronic relaxation process to become slower by enhancing intermediate excited-state lifetimes. While all of the compounds exhibit an ultrafast relaxation time scale, it increases from 34.1 ± 0.4 fs in ATT to 93.8 ± 0.6 fs in ATTO and is further increased to 117.8 ± 0.8 fs in ATTO$_2$. ANATz has an intermediate relaxation time scale of 39.8 ± 0.5 fs. The O substitution causes a relatively small change in the lifetime of the initially generated excitation. Instead, the longer relaxation time is due to a substantial increase in the lifetime of intermediate states caused by the larger energy gap between the excitation generated at 355 nm and lowest-energy state S$_1$ that is shifted to a lower energy in O-substituted compounds. The increased energy gap reduces the level of coupling between electronic states, leading to slower relaxation. The relaxation time scale is a measure of the rate at which the population is transferred to the S$_1$ state, which is also the state

where photochemistry occurs. Therefore, the slower electronic relaxation indicates that photodecomposition will also be slower for O-substituted compounds.

In terms of photochemistry, the bicyclic structure displays an increased QY compared to that of the single tetrazine ring. While the single-ring ANATz compound undergoes photo-dissociation only on the side chains with a QY of 50.8%, the bicyclic ring structure of the ATT and $ATTO_X$ compounds allows photodissociation of the ring framework and the total QY increases up to 94.0%. The photochemical QY weakly increases for each additional O substitution (ATT < ATTO < $ATTO_2$) as the number of possible pathways increases. It is relevant to point out that the energy-conserving Newtonian dynamics is essential for capturing all possible pathways by maximally exciting coupled vibrational motions to allow bonds to break. However, because all of the electronic energy is transferred to vibrations without any dissipation, the quantum yields reported here are overestimated. This analysis primarily considers the first bond dissociation step because subsequent reactions involving intermediates and fragments are limited by the closed-shell implementation of NEXMD, which prohibits nonsinglet configurations. An open-shell[32,37] implementation incorporating unpaired electrons would allow fragments (including radicals) that can change the subsequent photo-products and their ratios or introduce additional photo-chemical pathways. However, this is not expected to significantly affect the initial bond breaking steps reported here.

In conclusion, we have shown that it is possible to controllably manipulate the molecular structure of conjugated energetic materials through O substitution or a change in the ring framework to achieve a desired photochemical response. Despite the modest increase in the overall photochemical QY, O substitution introduces photodissociation pathways that always involve the functionalized site, revealing a reliable chemical modification for targeting specific photochemical functionality. Enhancing photochemical pathways through the addition of O on tetrazine and tetrazole rings appears to be an effective strategy.

ASSOCIATED CONTENT

Supporting Information

The Supporting Information is available free of charge on the ACS Publications website at DOI: 10.1021/acs.jpca.8b04381.

Contribution of excited states to computed absorption spectra, relaxation time scales and energy gaps for vacuum calculations, and dissociation reactions for ATT, ATTO, and $ATTO_2$ (PDF)

Movie files of representative trajectories for each molecule (ZIP)

AUTHOR INFORMATION

Corresponding Author
*E-mail: tammien@lanl.gov.

ORCID
Yu Zhang: 0000-0001-8938-1927
Sergei Tretiak: 0000-0001-5547-3647
Tammie Nelson: 0000-0002-3173-5291

Notes
The authors declare no competing financial interest.

REFERENCES

(1) Bowden, M. D.; Knowles, S. L. A High-Energy Fibre-to-Fibre Connection for Direct Optical Initiation Systems. *Proc. SPIE* **2012**, *8530*, 853016−853016−13.

(2) Moore, D. S.; Akinci, A. A.; Giambra, A. M.; Clarke, S. A.; Elert, M.; Furnish, M. D.; Anderson, W. W.; Proud, W. G.; Butler, W. T. Plasmonic Enhancement of Direct Optical Initiation of Explosives. *AIP Conf. Proc.* **2009**, *1195*, 161−164.

(3) Bykhalo, A. I.; Zhuzhukalo, E. V.; Kovalskii, N. G.; Kolomiiskii, A. N.; Korobov, V. V.; Rozhkov, A. D.; Yudin, A. I. Initiation of PETN by High-Power Laser Radiation. *Combust., Explos. Shock Waves* **1985**, *21*, 481−483.

(4) Tarzhanov, V. I.; Zinchenko, A. D.; Sdobnov, V. I.; Tokarev, B. B.; Pogrebov, A. I.; Volkova, A. A. Laser Initiation of PETN. *Combust., Explos. Shock Waves* **1996**, *32*, 454−459.

(5) Aluker, E. D.; Krechetov, A. G.; Mitrofanov, A. Y.; Nurmukhametov, D. R. Photochemical and Photothermal Dissocia-tion of PETN During Laser Initiation. *Russ. J. Phys. Chem. B* **2011**, *5*, 658−660.

(6) Greenfield, M. T.; McGrane, S. D.; Bolme, C. A.; Bjorgaard, J. A.; Nelson, T. R.; Tretiak, S.; Scharff, R. J. Photoactive High Explosives: Linear and Nonlinear Photochemistry of Petrin Tetrazine Chloride. *J. Phys. Chem. A* **2015**, *119*, 4846−4855.

(7) Greenfield, M. T.; McGrane, S. D.; Brown, K. E.; Moore, D. S.; Scharff, R. J. Towards Optical Control of Energetic Materials. *Fifteenth International Detonation Symposium*; Office of Naval Research: San Fransisco, 2014; pp 273−283.

(8) Nelson, T.; Bjorgaard, J. A.; Greenfield, M.; Bolme, C.; Brown, K.; McGrane, S.; Scharff, R. J.; Tretiak, S. Ultrafast Photodissociation Dynamics of Nitromethane. *J. Phys. Chem. A* **2016**, *120*, 519−526.

(9) Bjorgaard, J. A.; Sifain, A. E.; Nelson, T.; Myers, T. W.; Veauthier, J. M.; Chavez, D. E.; Scharff, R. J.; Tretiak, S. Two-Photon Absorption in Conjugated Energetic Molecules. *J. Phys. Chem. A* **2016**, *120*, 4455−4464.

(10) Wei, H.; Zhang, J.; Shreeve, J. M. Synthesis, Characterization, and Energetic Properties of 6-Aminotetrazolo[1,5-b]-1,2,4,5-tetrazine-7-N-oxide: A Nitrogen-Rich Material with High Density. *Chem. - Asian J.* **2015**, *10*, 1130−1132.

(11) Schulze, M. C.; Scott, B. L.; Chavez, D. E. A High Density Pyrazolo-triazine Explosive (PTX). *J. Mater. Chem. A* **2015**, *3*, 17963−17965.

(12) Chavez, D. E.; Bottaro, J. C.; Petrie, M.; Parrish, D. A. Synthesis and Thermal Behavior of a Fused, Tricyclic 1,2,3,4-Tetrazine Ring System. *Angew. Chem., Int. Ed.* **2015**, *54*, 12973−12975.

(13) Yin, P.; Shreeve, J. M. From N-Nitro to N-Nitroamino: Preparation of High-Performance Energetic Materials by Introducing Nitrogen-Containing Ions. *Angew. Chem.* **2015**, *127*, 14721−14725.

(14) Badaeva, E. A.; Timofeeva, T. V.; Masunov, A. M.; Tretiak, S. Role of Donor-Acceptor Strengths and Separation on the Two-Photon Absorption Response of Cytotoxic Dyes: a TD-DFT Study. *J. Phys. Chem. A* **2005**, *109*, 7276−7284.

(15) Morone, M.; Beverina, L.; Abbotto, A.; Silvestri, F.; Collini, E.; Ferrante, C.; Bozio, R.; Pagani, G. A. Enhancement of Two-Photon Absorption Cross-Section and Singlet-Oxygen Generation in Porphyrins upon -Functionalization with DonorAcceptor Substituents. *Org. Lett.* **2006**, *8*, 2719−2722.

(16) Nelson, T.; Fernandez-Alberti, S.; Chernyak, V.; Roitberg, A. E.; Tretiak, S. Nonadiabatic Excited-State Molecular Dynamics Modeling of Photoinduced Dynamics in Conjugated Molecules. *J. Phys. Chem. B* **2011**, *115*, 5402−5414.

(17) Nelson, T.; Fernandez-Alberti, S.; Chernyak, V.; Roitberg, A.; Tretiak, S. Nonadiabatic Excited-State Molecular Dynamics: Numerical Tests of Convergence and Parameters. *J. Chem. Phys.* **2012**, *136*, 054108.

(18) Fernandez-Alberti, S.; Roitberg, A.; Nelson, T.; Tretiak, S. Identification of Unavoided Crossings in Nonadiabatic Photoexcited Dynamics Involving Multiple Electronic States in Polyatomic Conjugated Molecules. *J. Chem. Phys.* **2012**, *137*, 014512.

(19) Nelson, T.; Fernandez-Alberti, S.; Roitberg, A. E.; Tretiak, S. Nonadiabatic Excited-State Molecular Dynamics: Treatment of Electronic Decoherence. *J. Chem. Phys.* **2013**, *138*, 224111.

(20) Nelson, T.; Fernandez-Alberti, S.; Roitberg, A. E.; Tretiak, S. Nonadiabatic Excited-State Molecular Dynamics: Modeling Photophysics in Organic Conjugated Materials. *Acc. Chem. Res.* **2014**, *47*, 1155−1164.

(21) Sifain, A. E.; Bjorgaard, J. A.; Nelson, T. R.; Nebgen, B. T.; White, A. J.; Gifford, B. J.; Gao, D. W.; Prezhdo, O. V.; Fernandez-Alberti, S.; Roitberg, A. E.; Tretiak, S. Photoexcited Nonadiabatic Dynamics of Solvated Push-Pull π-Conjugated Oligomers with the NEXMD Software. *J. Chem. Theory Comput.* **2018**, n/a.

(22) Tully, J. Molecular Dynamics with Electronic Transitions. *J. Chem. Phys.* **1990**, *93*, 1061−1071.

(23) Tavernelli, I.; Curchod, B. F. E.; Laktionov, A.; Rothlisberger, U. Nonadiabatic Coupling Vectors for Excited States within Time-Dependent Density Functional Theory in the Tamm-Dancoff Approximation and Beyond. *J. Chem. Phys.* **2010**, *133*, 194104.

(24) Furche, F. On the Density Matrix Based Approach to Time-Dependent Density Functional Response Theory. *J. Chem. Phys.* **2001**, *114*, 5982−5992.

(25) Furche, F.; Ahlrichs, R. Adiabatic Time-Dependent Density Functional Methods for Excited State Properties. *J. Chem. Phys.* **2002**, *117*, 7433−7447.

(26) Tretiak, S.; Chernyak, V.; Mukamel, S. Recursive Density-Matrix-Spectral-Moment Algorithm for Molecular Nonlinear Polarizabilities. *J. Chem. Phys.* **1996**, *105*, 8914−8928.

(27) Tretiak, S.; Isborn, C.; Niklasson, A.; Challacombe, M. Representation Independent Algorithms for Molecular Response Calculations in Time-Dependent Self-Consistent Field Theories. *J. Chem. Phys.* **2009**, *130*, 054111.

(28) Chernyak, V.; Schulz, M. F.; Mukamel, S.; Tretiak, S.; Tsiper, E. V. Krylov-Space Algorithms for Time-Dependent Hartree-Fock and Density Functional Computations. *J. Chem. Phys.* **2000**, *113*, 36−43.

(29) Thouless, D. J. *The Quantum Mechanics of Many-Body Systems*; Academic Press: New York, 1972.

(30) Dewar, M. J. S.; Zoebisch, E. G.; Healy, E. F.; Stewart, J. J. P. AM1: A New General Purpose Quantum Mechanical Molecular Model. *J. Am. Chem. Soc.* **1985**, *107*, 3902−3909.

(31) Hirata, S.; Head-Gordon, M.; Bartlett, R. J. Configuration Interaction Singles, Time-Dependent Hartree-Fock, and Time-Dependent Density Functional Theory for the Electronic Excited States of Extended Systems. *J. Chem. Phys.* **1999**, *111*, 10774−10786.

(32) Vincent, J. C.; Muuronen, M.; Pearce, K. C.; Mohanam, L. N.; Tapavicza, E.; Furche, F. That Little Extra Kick: Nonadiabatic Effects in Acetaldehyde Photodissociation. *J. Phys. Chem. Lett.* **2016**, *7*, 4185−4190.

(33) Tapavicza, E.; Bellchambers, G. D.; Vincent, J. C.; Furche, F. Ab Initio Non-Adiabatic Molecular Dynamics. *Phys. Chem. Chem. Phys.* **2013**, *15*, 18336−18348.

(34) Neukirch, A. J.; Shamberger, L. C.; Abad, E.; Haycock, B. J.; Wang, H.; Ortega, J.; Prezhdo, O. V.; Lewis, J. P. Nonadiabatic Ensemble Simulations of cis-Stilbene and cis-Azobenzene Photoisomerization. *J. Chem. Theory Comput.* **2014**, *10*, 14−23.

(35) Han, Y.; Meng, Q.; Rasulev, B.; May, P. S.; Berry, M. T.; Kilin, D. S. Photofragmentation of the Gas-Phase Lanthanum Isopropylcyclopentadienyl Complex: Computational Modeling vs Experiment. *J. Phys. Chem. A* **2015**, *119*, 10838−10848.

(36) Han, Y.; Meng, Q.; Rasulev, B.; May, P. S.; Berry, M. T.; Kilin, D. S. Photoinduced Charge Transfer versus Fragmentation Pathways in Lanthanum Cyclopentadienyl Complexes. *J. Chem. Theory Comput.* **2017**, *13*, 4281−4296.

(37) Han, Y.; Rasulev, B.; Kilin, D. S. Photofragmentation of Tetranitromethane: Spin-Unrestricted Time-Dependent Excited-State Molecular Dynamics. *J. Phys. Chem. Lett.* **2017**, *8*, 3185−3192.

(38) Coe, J. D.; Levine, B. G.; Martinez, T. J. Ab Initio Molecular Dynamics of Excited-State Intramolecular Proton Transfer Using Multireference Perturbation Theory. *J. Phys. Chem. A* **2007**, *111*, 11302−11310.

(39) Worth, G. A.; Meyer, H.-D.; Köppel, H.; Cederbaum, L. S.; Burghardt, I. Using the MCTDH Wavepacket Propagation Method to Describe Multimode Non-Adiabatic Dynamics. *Int. Rev. Phys. Chem.* **2008**, *27*, 569−606.

(40) Bjorgaard, J. A.; Kuzmenko, V.; Velizhanin, K.; Tretiak, S. Solvent Effects in Time-Dependent Self-Consistent Field Methods. I. Optical Response Calculations. *J. Chem. Phys.* **2015**, *142*, 044103.

(41) Bjorgaard, J. A.; Velizhanin, K. A.; Tretiak, S. Solvent Effects in Time-Dependent Self-Consistent Field Methods. II. Variational Formulations and Analytical Gradients. *J. Chem. Phys.* **2015**, *143*, 054305.

(42) Bjorgaard, J. A.; Nelson, T.; Kalinin, K.; Kuzmenko, V.; Velizhanin, K. A.; Tretiak, S. Simulations of Fluorescence Solvatochromism in Substituted PPV Oligomers from Excited State Molecular Dynamics with Implicit Solvent. *Chem. Phys. Lett.* **2015**, *631−632*, 66−69.

(43) Bjorgaard, J. A.; Velizhanin, K. A.; Tretiak, S. Nonequilibrium Solvent Effects in Born-Oppenheimer Molecular Dynamics for Ground and Excited Electronic States. *J. Chem. Phys.* **2016**, *144*, 154104.

(44) Tomasi, J.; Mennucci, B.; Cammi, R. Quantum Mechanical Continuum Solvation Models. *Chem. Rev.* **2005**, *105*, 2999−3094.

(45) Klamt, A.; Schüürmann, G. COSMO: A New Approach to Dielectric Screening in Solvents with Explicit Expressions for the Screening Energy and its Gradient. *J. Chem. Soc., Perkin Trans. 2* **1993**, *2*, 799−805.

(46) Paterlini, M.; Ferguson, D. Constant Temperature Simulations using the Langevin Equation with Velocity Verlet Integration. *Chem. Phys.* **1998**, *236*, 243−252.

(47) Stewart, J. J. P. *MOPAC 2016*; Stewart Computational Chemistry: Colorado Springs, CO, 2016.

(48) Armstrong, D. R.; Perkins, P. G.; Stewart, J. J. P. Bond Indices and Valency. *J. Chem. Soc., Dalton Trans.* **1973**, 838−840.

(49) Cottrell, T. L. *The Strengths of Chemical Bonds*, 2nd ed.; Butterworths Scientific Publications: London, 1958; pp A-21−A-34.

(50) deB. Darwent, B. *National Standard Reference Data Series*; National Bureau of Standards: Washington, DC, 1970; Vol. *31*.

(51) Benson, S. W. III - Bond Energies. *J. Chem. Educ.* **1965**, *42*, 502.